

---

# COOPERATIVE LONG ROPE SKIPPING VIA MULTI-AGENT REINFORCEMENT LEARNING

---

A PREPRINT

Zihao Wang<sup>1,2</sup>, Shijie Peng<sup>2</sup>, Kerui Wu<sup>2</sup>, Yu Huang<sup>2</sup>, Ruiqi Xue<sup>1,2</sup>,  
Dong Liu<sup>3</sup>, Tian Xu<sup>1,2</sup>, Lei Yuan<sup>1,2</sup>, Yang Yu<sup>1,2</sup>

<sup>1</sup> National Key Laboratory of Novel Software Technology, Nanjing University, Nanjing, China

<sup>2</sup> School of Artificial Intelligence, Nanjing University, Nanjing, China

<sup>3</sup> Beijing Academy of Artificial Intelligence, BAAI, Beijing, China

{wangzh, xuerq, xut, yuanl, yuy}@lamda.nju.edu.cn,

{pengsj, wukerui, huangy}@smail.nju.edu.cn, liudong@baai.ac.cn

## ABSTRACT

Humans exhibit remarkable motor agility, enabling a wide range of dynamic skills such as running and jumping, which highlights the great potential of humanoid robots for athletic locomotion. Among athletic sports, long rope skipping requires two rope turners to cooperatively swing the rope while adapting to a player under different jumping rhythms, making it a meaningful yet challenging task for humanoid robots. Although existing methods for humanoid sports have achieved success in single-agent and interaction-free settings, such as running, dancing, and parkour, task scenarios that require precise coordination among multiple participants remain largely unexplored. To this end, we propose Marope, a multi-agent reinforcement learning (MARL) framework for cooperative long rope skipping with multiple humanoid robots. Specifically, Marope adopts a hierarchical reinforcement learning framework for policy training. At the lower level, it learns decentralized rope manipulation policies through MARL, while at the upper level, a centralized scheduling policy is trained to coordinate the execution of the lower-level policies. To improve generalization across different player behavioral styles, Marope further incorporates diverse jumping policies into cooperative game training. We evaluate our approach on Unitree G1 humanoid robots in both simulation and real-world settings. Experimental results demonstrate that Marope outperforms various baselines, achieving more efficient and stable rope manipulation as well as more robust and adaptable cooperation with varied players. More results can be found on the project website: <https://marope-dev.github.io/>.

## 1 Introduction

Developing humanoid robots capable of emulating agile and robust human motions across diverse and complex environments has long been a central goal of embodied intelligence [Hirai et al.(1998), Tong et al.(2024), He et al.(2024)]. Within this broader pursuit, research on humanoid sports [Crowley et al.(2023), Qi et al.(2023), Qin et al.(2018), Zhuang et al.(2025), Su et al.(2025)] has emerged as a particularly active direction, driven by the widespread popularity and unique recreational value of sports in human life, as well as the strong demands they impose on versatile and dynamic whole-body control. Among these sports, long rope skipping is a widely practiced recreational activity, valued for its highly social nature which requires multiple participants and its benefits for physical fitness. Enabling humanoids to participate in long rope skipping therefore presents an important yet challenging research problem.

Although humanoid sports have received increasing attention, most existing studies focus on single-agent task settings, where a centralized learning framework is employed to control an individual humanoid for an isolated athletic skill. However, long rope skipping departs from this formulation in several fundamental aspects. First, the task requires two humanoid rope turners to generate a coherent rope motion through whole-body control, while maintaining balance and stable foot contacts. Second, the rope is a deformable and underactuated object whose intermediate configuration cannot be directly controlled [Liu et al.(2023)], making simple trajectory replay [Bruce et al.(2017), Di Palo and Johns(2024)] or blind motion tracking [Thuruthel et al.(2018), Liao et al.(2025)] insufficient for reliable rope manipulation. Third,

successful skipping depends on precise temporal synchronization between the rope rotation phase and the player’s jumping phase; even small phase mismatches may result in rope-player collisions or failed jumps. In open-world cooperative scenarios, this challenge becomes even more pronounced, as players may exhibit diverse and unknown behavioral styles [Yuan et al.(2023)]. Therefore, cooperative long rope skipping calls for a learning framework that can coordinate multiple humanoids, manipulate a flexible rope in a closed loop and adapt to diverse jumping behaviors.

To address these challenges, we propose Marope, a multi-humanoid cooperative reinforcement learning (RL) framework for long rope skipping that can adapt to diverse rope jumping patterns. Specifically, Marope first pretrains a decentralized rope manipulation policy for two humanoid rope turners with MAPPO under the CTDE paradigm, using a compact command space that specifies the rotation center and rotation angular velocity instead of prescribing full rope trajectories. Built on this reusable low-level skill, Marope learns a centralized scheduling policy to dynamically adjust the manipulation commands to synchronize with a player’s jumping rhythm while reducing rope-player collisions. To improve robustness to different partners, Marope further trains a latent-conditioned jumping policy with an IPM-based diversity intrinsic objective and uses the resulting diverse behaviors for data augmentation, encouraging the scheduling policy to generalize across varied jumping styles. We evaluate our approach on Unitree G1 humanoid robots in both simulation and real-world environments. Experimental results demonstrate that our method outperforms various baselines, and produces more efficient and stable rope manipulation as well as more robust and adaptable cooperation with diverse players. To the best of our knowledge, this work presents the first multi-humanoid cooperative long rope skipping system, extending humanoid sports from single-agent athletic skills to tightly coordinated multi-robot scenarios.

## 2 Related Work

**Learning-based Humanoid Control** Learning-based methods have substantially advanced humanoid control, particularly in robust locomotion and sim-to-real transfer. Early works focused on stable and versatile bipedal locomotion, including walking, running, velocity tracking, and terrain adaptation [Li et al.(2019), Li et al.(2021), Radosavovic et al.(2024a), Radosavovic et al.(2024b), Long et al.(2025)]. Recent benchmarks and systems further extend humanoid control toward high-dimensional whole-body tasks, highlighting both the promise and challenges of learning general-purpose humanoid behaviors [Sferrazza et al.(2024)]. Meanwhile, motion imitation and teleoperation have enabled humanoid robots to acquire expressive whole-body skills from human motion data or demonstrations, such as dancing, gesturing, dexterous teleoperation, and dynamic motion tracking [Liao et al.(2025), Cheng et al.(2024), Ji et al.(2025), He et al.(2025)]. Building on these advances, humanoid sports have emerged as a compelling testbed for agile whole-body control. Prior work has explored vertical jumping, parkour, table tennis, badminton, and tennis, demonstrating increasingly dynamic interactions with environments, objects, and human players [Qi et al.(2023), Zhuang et al.(2025), Su et al.(2025), Chen et al.(2026), Zhang et al.(2026)]. However, most methods are formulated as single-humanoid control problems, where one policy controls an individual robot to perform an athletic skill or react to external objects. In contrast, long rope skipping requires multiple humanoids to coordinate whole-body motions through a shared deformable rope while synchronizing with a jumping participant.

**Multi-agent Reinforcement Learning** Multi-agent Reinforcement Learning (MARL) utilizes RL to address multi-agent problems. Unlike single-agent settings, MARL faces the curse of dimensionality in the joint state-action space, which stems from the growing number of agents. To overcome this challenge, typical works utilize value decomposition [Sunehag et al.(2017), Rashid et al.(2018)] or decentralized policy gradient [Lowe et al.(2017), Wang et al.(2021), Yu et al.(2022)] to transform the complex high-dimensional joint space into tractable low-dimensional representations, demonstrating high learning efficiency in fields such as autonomous driving [Zhang et al.(2024)], financial trading [Fang et al.(2023)], and embodied intelligence [Feng et al.(2026)]. In addition to the aforementioned methods and their variants, many other research directions have been explored in MARL, including efficient communication mechanisms for mitigating partial observability under decentralized policy execution [Zhu et al.(2022)], offline policy learning [Zhang et al.(2023)], world models for MARL [Wang et al.(2022)], and policy robustness in the presence of perturbations [Guo et al.(2022)].

## 3 Preliminaries

We formalize the cooperative long rope skipping problem as a Partially Observable Markov Game  $\mathcal{M} = \langle \mathcal{N}, \mathcal{S}, \{\mathcal{A}^i\}_{i \in \mathcal{N}}, P, \{R^i\}_{i \in \mathcal{N}}, \gamma, \{\Omega^i\}_{i \in \mathcal{N}}, \mathcal{O} \rangle$ , where  $\mathcal{N} = \{1, 2, \dots, n\}$  represents the set of participant agents,  $\mathcal{S}$  is the global state space,  $\mathcal{A}^i$  and  $\Omega^i$  are the action and observation spaces of agent  $i$ . At timestep  $t$  with global state  $s_t \in \mathcal{S}$ , each agent  $i$  observes a partial observation  $o_t^i \in \Omega^i$  according to the observation probability  $O(\cdot | s_t, i)$  and chooses an action  $a_t^i$ . After executing the joint action  $\mathbf{a}_t = \{a_t^i\}_{i \in \mathcal{N}}$ , each agent  $i$  will receive a reward  $r_t^i = R^i(s_t, \mathbf{a}_t)$

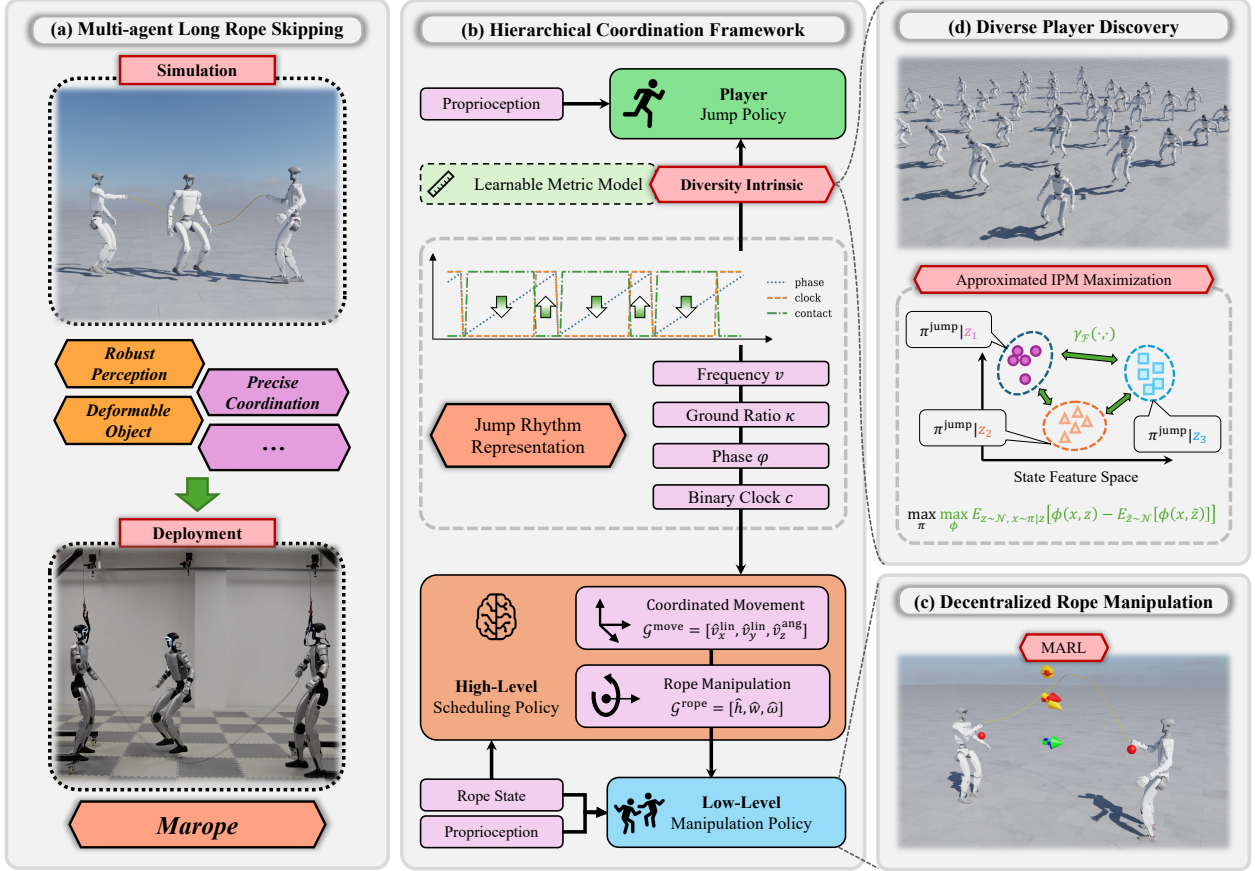


Figure 1: **Overview of Marope.** (a) For long rope skipping task, Marope builds a pipeline for learning long rope skipping skills on multiple humanoid robots (b) A hierarchical coordination framework is used for efficient coordination with player under specific jump rhythm. (c) The low-level decentralized rope manipulation policy is trained via MARL. (d) Through an IPM-based diversity intrinsic objective, diverse player behaviors are discovered to improve generality of high-level scheduling policy.

and the global state will transit to  $s_{t+1} \sim P(s_{t+1} | s_t, \mathbf{a}_t)$ . The goal of each agent  $i$  is to learn a policy  $\pi^i(a_t^i | o_t^i)$  that maximizes its expected return  $\mathbb{E} [\sum_{t=0}^{\infty} \gamma^t r_t^i]$  under discounted factor  $\gamma \in [0, 1)$ .

## 4 Method

This section gives the detailed Marope, a novel framework for learning cooperative long rope skipping. Section 4.1 presents the formulation and decentralized training of the low-level rope manipulation policy, Section 4.2 introduces rhythm representation and training of the high-level centralized scheduling policy, while Section 4.3 describes how Marope discovers diverse player behavior with a diversity intrinsic objective to improve policy generalization and adaptability.

### 4.1 Decentralized Cooperative Rope Manipulation

Rope manipulation is the foundation of the long rope skipping, thus, we first pretrain a decentralized cooperative rope manipulation policy  $\pi^{\text{manip}}(a_t | o_t^{\text{manip}})$  for two humanoid rope turners. The core objective is to rotate the rope around a reference center  $\mathbf{p}^c$  under a target angular velocity  $\hat{\omega}$ .

**Rope Manipulation Modeling** Specifically, let  $\mathbf{p}_{\text{base}}^1$  and  $\mathbf{p}_{\text{base}}^2$  denote the base link positions of two humanoid rope turners, we define the reference center  $\mathbf{p}^c$  and rotation axis  $\mathbf{e}^r$  as follows:

$$\mathbf{p}^c = \Pi_{xy} \left( \frac{\mathbf{p}_{\text{base}}^1 + \mathbf{p}_{\text{base}}^2}{2} \right) + [0, 0, \hat{h}]^\top, \quad \mathbf{e}^r = \frac{\Pi_{xy}(\mathbf{p}_{\text{base}}^2 - \mathbf{p}_{\text{base}}^1)}{\|\Pi_{xy}(\mathbf{p}_{\text{base}}^2 - \mathbf{p}_{\text{base}}^1)\|_2}, \quad (1)$$

where the horizontal projection operator  $\Pi_{xy}([x, y, z]^\top) = [x, y, 0]^\top$ ,  $\hat{h}$  is the target rotation height. The target rotation angular velocity can be further given as  $\hat{\omega} = \hat{\omega} \cdot \mathbf{e}^r$  via a signed scalar  $\hat{\omega}$ . This definition guarantees SE(2) mobility for the rope manipulation behavior, enabling the humanoid rope turners to swing the rope while simultaneously translating, turning, and repositioning.

Accordingly, we design the command as  $\mathcal{G}^{\text{manip}} = [\mathcal{G}^{\text{move}}, \mathcal{G}^{\text{rope}}]$ , including coordinated movement related components  $\mathcal{G}^{\text{move}} = [\hat{v}_x^{\text{lin}}, \hat{v}_y^{\text{lin}}, \hat{v}_z^{\text{ang}}]$  and rope manipulation related components  $\mathcal{G}^{\text{rope}} = [\hat{h}, \hat{w}, \hat{\omega}]$ , where  $\hat{v}_x^{\text{lin}}, \hat{v}_y^{\text{lin}}, \hat{v}_z^{\text{ang}}$  refer to the target linear and angular velocity of the reference center and rotation axis in the world frame,  $\hat{w}$  is the target width for two rope ends. Compared with explicitly specifying reference trajectories for a deformable object, the above abstraction provides a compact description for the key rope motion pattern in the long rope skipping task:  $\hat{v}_x^{\text{lin}}, \hat{v}_y^{\text{lin}}, \hat{v}_z^{\text{ang}}$  control the overall stances,  $\hat{h}$  and  $\hat{w}$  constrain the region swept by rope, whereas  $\hat{\omega}$  specifies the swinging rhythm.

**Symmetric Observation Construction** Given the modeling above, the observation of the rope manipulation policy on humanoid rope turner  $i \in \{1, 2\}$  comprises three parts: command observation  $o_t^{\text{cmd},i}$ , rope morphology history  $o_{t-H+1:t}^{\text{rope},i}$  and proprioceptive sensing history  $o_{t-H+1:t}^{\text{proprio},i}$ . For simplicity, we omit the subscript  $t$  in the following detailed explanation. The command observation is computed as  $o^{\text{cmd},i} = [\hat{v}_x^{\text{lin},i}, \hat{v}_y^{\text{lin},i}, \hat{v}_z^{\text{ang}}, \hat{h}, \hat{w}, \text{sign}(i) \cdot \hat{\omega}]$ , where the target linear velocity of the reference center ( $\hat{v}_x^{\text{lin},i}, \hat{v}_y^{\text{lin},i}$ ) is represented in the yaw-only base link frame of humanoid rope turner  $i$ , the target rotation angular velocity  $\hat{\omega}$  is multiplied with  $\text{sign}(i) = \begin{cases} +1 & i = 1 \\ -1 & i = 2 \end{cases}$  to ensure the symmetry.

The rope morphology  $o^{\text{rope},i} = [\mathbf{p}^{\text{rope},i}[k_1^i], \mathbf{p}^{\text{rope},i}[k_2^i], \dots, \mathbf{p}^{\text{rope},i}[k_m^i]]$  concatenates positions of  $m$  points within the discretely simulated rope, which are represented in the base link frame of humanoid rope turner  $i$ . The observing indices  $k_{1:m}^i$  are randomly sampled at the start of the episode and ordered by their index distance to the rope end attached on humanoid rope turner  $i$ . The proprioceptive sensing  $o^{\text{proprio},i} = [\omega^{\text{b}}, \mathbf{g}^{\text{b}}, \mathbf{q}, \dot{\mathbf{q}}, \hat{a}]$  contains base link angular velocity  $\omega^{\text{b}}$ , gravity projected in the base link frame  $\mathbf{g}^{\text{b}}$ , joint positions  $\mathbf{q}$ , joint velocities  $\dot{\mathbf{q}}$  and action at last timestep  $\hat{a}$ .

**Multi-Agent Policy Optimization** Finally, with the above observations, the policy outputs action  $a_t \in \mathbb{R}^{N_{\text{joints}}}$  to further derive the target joint positions of all joints  $\hat{\mathbf{q}}_t = \mathbf{q}_{\text{default}} + \alpha \odot a_t$  for PD controller [Liao et al.(2025)]. To ensure real-time decentralized inference, we adopt the Multi-Agent Proximal Policy Optimization (MAPPO) [Yu et al.(2022)] algorithm with Centralized Training and Decentralized Execution (CTDE) paradigm to optimize  $\pi^{\text{manip}}$  under the reward terms described in Appendix.

## 4.2 High-level Scheduling Policy

The aforementioned rope manipulation policy enables two humanoid robots to cooperatively control the rope. However, integrating this skill with a player to perform group long rope skipping remains unresolved. To address this issue, we further train a high-level scheduling policy  $\pi^{\text{sched}}$  to coordinate with a physically controlled humanoid player.

**Jump Rhythm Representation** First, to obtain a reliable jumping policy, we formally model the jumping task as an alternating process between ground and air stages. To be specific, each cycle in such process can be described as a tuple  $\mathcal{G}^{\text{rhythm}} = (\nu, \kappa, \varphi, c = \mathbf{1}(\varphi > \kappa))$ , where  $\nu = 1/T$  refers to the frequency induced by the cycle length  $T$ ,  $\kappa = T^{\text{ground}}/T$  represents the ratio of the ground stage and  $\varphi \in [0, 1)$  is a continuous phase variable indicating the progress within the cycle, which steps forward via  $\varphi \leftarrow \varphi + \nu\Delta t$  and is reset to 0 at the start of a new cycle.

**Jump Policy Training** Based on the clock signal, we train a jumping policy  $\pi^{\text{jump}}(a_t | o_t^{\text{jump}} = [\mathcal{G}^{\text{rhythm}}, o_{t-H+1:t}^{\text{proprio}}])$  to provide physically plausible jumping motions, where the action  $a_t$  and the proprioceptive sensing history  $o_{t-H+1:t}^{\text{proprio}}$  share the same definition as  $\pi^{\text{manip}}$ . The core objective of policy  $\pi^{\text{jump}}$  is to align the binary feet contact mask with the binary clock  $c$ , which can further derive the periodic jumping behavior as shown in Figure 1. Additional rewards can be found in Appendix.

**Centralized Scheduling** With the pretrained rope manipulation policy  $\pi^{\text{manip}}$ , we introduce the high-level scheduling policy  $\pi^{\text{sched}}(\mathcal{G}^{\text{manip}} \mid o_t^{\text{sched}})$  to adaptively adjust  $\mathcal{G}^{\text{manip}}$ . The observation is defined as  $o_t^{\text{sched}} = [\mathcal{G}^{\text{rhythm}}, o_{t-H+1:t}^{\text{rope}}, o_{t-H+1:t}^{\text{player}}]$ , where the player state  $o_t^{\text{player}} = [\mathbf{p}_t^{\text{obb}}, \mathbf{R}_t^{\text{obb}}, \Delta_t^{\text{obb}}]$  includes position  $\mathbf{p}_t^{\text{obb}}$ , orientation  $\mathbf{R}_t^{\text{obb}}$  and size  $\Delta_t^{\text{obb}}$  of the player Oriented Bounding Box (OBB). Both  $o_t^{\text{rope}}$  and  $o_t^{\text{player}}$  are represented in the rotation center frame. The core objective of policy  $\pi^{\text{sched}}$  is to synchronize with the player’s jumping rhythm while reducing the collision risk between the rope and the player. For rhythm synchronization, we first define the rope rotation phase around axis  $\mathbf{e}^r$  as

$$\bar{\theta}^{\text{rope}} = \frac{1}{2\pi N} \sum_{i=1}^N \text{atan2}(\text{sgn}(\langle \bar{\omega}, \mathbf{e}^r \rangle) \xi_i^y, -\xi_i^z), \quad (2)$$

$$\bar{\omega} = \arg \min_{\omega} \sum_{i=1}^N \|\mathbf{v}^{\text{rope}}[i] - \omega \times (\mathbf{p}^{\text{rope}}[i] - \mathbf{p}^c)\|_2^2, \quad \xi_i = [\mathbf{e}^r, \mathbf{e}^z \times \mathbf{e}^r, \mathbf{e}^z](\mathbf{p}^{\text{rope}}[i] - \mathbf{p}^c).$$

Ideally, the rotation phase  $\bar{\theta}^{\text{rope}}$  should periodically go through 0 when the player ascends to the highest points (i.e.,  $\varphi = 1 - \frac{1-\kappa}{2}$ ) in order to make successful rope skips. Thus, we set the target rotation phase  $\hat{\theta}^{\text{rope}}$  to be  $\frac{1-\kappa}{2}$  ahead of the jump rhythm phase  $\varphi$  and compute the phase tracking error along with the other reward terms listed in Appendix to optimize  $\pi^{\text{sched}}$ .

### 4.3 Diverse Player Discovery

The preceding scheduling policy  $\pi^{\text{sched}}$  enables the humanoid rope turners to coordinate with a fixed-style player. However, in practice, different individuals may possess various motion patterns. To enhance the adaptability of  $\pi^{\text{sched}}$  to such variations, we introduce an auxiliary intrinsic objective to discover diverse player behaviors, which are then used as counterparts in cooperative game training.

**Diversity Intrinsic Objective** To be specific, the jumping policy  $\pi^{\text{jump}}(a_t \mid o_t^{\text{jump}}, z)$  is conditioned on a continuous latent variable  $z \in \mathbb{R}^{d_{\text{latent}}}$  in addition to the original observations  $o_t^{\text{jump}}$ . To increase the discrepancy between states visited by policy with different latent  $z$ , we formulate a diversity intrinsic objective as follows:

$$\max_{\pi^{\text{jump}}} \gamma_{\mathcal{F}}(p(x, z), p(x)p(z)) = \sup_{f \in \mathcal{F}} \mathbb{E}_{z \sim p(z), x \sim \pi^{\text{jump}}(z)} [f(x, z) - \mathbb{E}_{\tilde{z} \sim p(z)} f(x, \tilde{z})], \quad (3)$$

where  $\gamma_{\mathcal{F}}(\cdot, \cdot)$  denotes Integral Probability Metric (IPM) over the function class  $\mathcal{F}$ ,  $x \in \mathbb{R}^{d_{\text{feat}}}$  is the feature variable describing the states visited by policy, e.g. local-frame end-effectors poses.

**Practical Implementation** We use a standard Gaussian distribution  $\mathcal{N}(\mathbf{0}, \mathbf{I}_{d_{\text{latent}}})$  as the prior latent distribution  $p(z)$ . We choose  $\mathcal{F}$  to be the set of 1-Lipschitz continuous functions in  $\mathbb{R}^{d_{\text{feat}}+d_{\text{latent}}}$ , which makes  $\gamma_{\mathcal{F}}(\cdot, \cdot)$  equivalent to Wasserstein-1 distance  $\mathcal{I}_{\mathcal{W}}(\cdot, \cdot)$ . Since directly searching in the whole function class  $\mathcal{F}$  is intractable, an extra learnable metric model  $\phi: \mathbb{R}^{d_{\text{feat}}+d_{\text{latent}}} \mapsto \mathbb{R}$  is optimized along with the policy  $\pi^{\text{jump}}$  to approximate the supremum in the IPM

$$\max_{\phi} \mathbb{E}_{z \sim p(z), x \sim \pi^{\text{jump}}(z)} [\phi(x, z) - \mathbb{E}_{\tilde{z} \sim p(z)} \phi(x, \tilde{z})], \quad (4)$$

where the Lipschitz continuity of  $\phi$  is guaranteed by applying Spectral Normalization [Miyato et al.(2018)]. The diversity intrinsic serves as an additional reward term weighted with the task rewards, forming a composite reward  $r_t^{\text{div}} = r_t^{\text{task}} + \beta \phi(x_t, z)$  for policy optimization. We also introduce a curriculum mechanism to enable diversity intrinsic only when the policy  $\pi^{\text{jump}}$  reaches a predefined task performance threshold, thereby restricting that diversity objective does not hinder the main task objectives.

## 5 Experiments

In this section, we conduct extensive experiments in both simulation and real-world settings to answer the following research questions: (1) Can Marope perform flexible and stable rope manipulation (Section 5.2)? (2) Can Marope efficiently cooperate with diverse players (Section 5.3)? (3) Can Marope robustly transfer to real-world scenarios (Section 5.4)?

Table 1: **Simulation Results of Rope Manipulation.**

	Metrics	Ours	Single Agent	Open Loop	w/o Segment Sampling
<b>Rope Manipulation</b>	$E_{\text{rot}} (\downarrow)$	<b>1.719 ± 0.332</b>	2.733 ± 0.539	6.754 ± 2.018	2.223 ± 0.484
	$E_{\text{wid}} (\downarrow)$	<b>0.063 ± 0.011</b>	0.136 ± 0.030	0.284 ± 0.135	0.087 ± 0.038
<b>Coordinated Movement</b>	$E_{\text{lin}} (\downarrow)$	<b>0.103 ± 0.011</b>	0.222 ± 0.052	0.199 ± 0.049	0.121 ± 0.024
	$E_{\text{ang}} (\downarrow)$	<b>0.109 ± 0.041</b>	0.114 ± 0.039	0.112 ± 0.040	0.110 ± 0.041
<b>Control Stability</b>	Act. Rate ( $\downarrow$ )	1.349 ± 0.130	1.526 ± 0.207	<b>0.945 ± 0.097</b>	1.300 ± 0.142
	Feet Slip. ( $\downarrow$ )	<b>0.040 ± 0.003</b>	0.122 ± 0.010	0.082 ± 0.012	0.053 ± 0.004

## 5.1 Experimental Settings

**Simulation Environment** We conduct our simulation experiments in Isaac Lab [Mittal et al.(2025)] for massive parallel simulation. To approximately simulate the physical properties of a rope, we create  $N$  small rigid capsules and connect them via passively driven spherical joints. Each end of the rope is attached to the wrist link of the corresponding humanoid rope turner with hand removed.

**Real-world Deployment** We deploy Marope on Unitree G1 29-dof humanoid robots. An optical motion capture (MoCap) system is utilized to obtain (a) positions of  $m$  reflective markers affixed to the rope (b) poses of base links in humanoid rope turners (c) positions of key body parts of the player, which are transported to each computing node for observation construction.

## 5.2 Rope Manipulation Analysis

**Baselines** We first evaluate the effectiveness of the rope manipulation component of Marope and compare it with several baselines defined as follows: (1) **Single Agent** uses a single-agent policy to control two humanoids simultaneously, where the observation input and action output are formed by concatenating the observations and actions of our policy, i.e.,  $[o_t^{\text{manip},1}, o_t^{\text{manip},2}]$  and  $[a_t^1, a_t^2]$ ; (2) **Open Loop** records the evaluation trajectories of our policy and then reproduces the motion independently on each humanoid using a motion tracking method [Liao et al.(2025)]; while (3) **w/o Segment Sampling** uses uniformly spaced rope observation indices instead of randomly sampled ones during training.

**Metrics** In the comparison, we evaluate the performance of rope manipulation using the following metrics: (1) **Rotation Tracking Error**  $E_{\text{rot}} = \mathbb{E}[\|\hat{\omega} - \hat{\omega}\|_2]$ ; (2) **Width Tracking Error**  $E_{\text{wid}} = \mathbb{E}[|w - \hat{w}|]$ ; (3) **Linear Velocity Tracking Error**  $E_{\text{lin}} = \mathbb{E}[\|v_{xy}^{\text{lin}} - \hat{v}_{xy}^{\text{lin}}\|_2]$ ; (4) **Angular Velocity Tracking Error**  $E_{\text{ang}} = \mathbb{E}[\|v_z^{\text{ang}} - \hat{v}_z^{\text{ang}}\|]$ ; (5) **Action Rate**, which measures the difference between actions at adjacent timesteps; and (6) **Feet Slippage**, defined as the horizontal sliding velocity of the feet when they are in contact with the ground. Metrics (1)–(4) evaluate task completion performance, while (5)–(6) measure the control stability. All metrics are estimated over 1,000 episodes.

**Comparison Results** The experimental results are presented in Table 1. First, Single Agent performs consistently worse than our method across all metrics, suggesting that modeling the task as a single-agent control problem introduces redundant and highly coupled observation-action spaces, thereby reducing optimization efficiency. Second, Open Loop achieves slightly smoother actions, but its rope manipulation accuracy drops substantially, highlighting the limitations of blind motion tracking in handling the complex deformable object dynamics involved in rope turning and demonstrates the necessity of closed-loop reinforcement learning. Finally, w/o Segment Sampling shows mild degradation in both rope manipulation and coordinated-movement metrics, indicating weaker robustness to disturbances from randomly spaced rope observation points, which more closely resemble real-world sensing conditions. Taken together, these results validate the effectiveness of our module designs for low-level rope manipulation.

## 5.3 Player Coordination Analysis

**Baselines and Metrics** We then evaluate the cooperative rope skipping performance of Marope and the baseline methods with a diverse jumping policy conditioned on randomly sampled latent codes in simulation. The baselines include (1) **w/o Scheduling**, which disables the high-level scheduling policy and instead uses the clock frequency to

Table 2: **Simulation Results of Player Coordination.**

Metrics	Ours	w/o Scheduling	w/o Player Diversity
Overlap Ratio ( $\downarrow$ )	<b>0.090 <math>\pm</math> 0.049</b>	0.392 $\pm$ 0.140	0.120 $\pm$ 0.094
Phase Tracking Error ( $\downarrow$ )	<b>0.397 <math>\pm</math> 0.115</b>	1.092 $\pm$ 0.273	0.414 $\pm$ 0.155
Player Tracking Error ( $\downarrow$ )	<b>0.116 <math>\pm</math> 0.022</b>	0.182 $\pm$ 0.360	0.172 $\pm$ 0.021
Complete Rate ( $\uparrow$ )	<b>0.787 <math>\pm</math> 0.204</b>	0.358 $\pm$ 0.207	0.751 $\pm$ 0.216

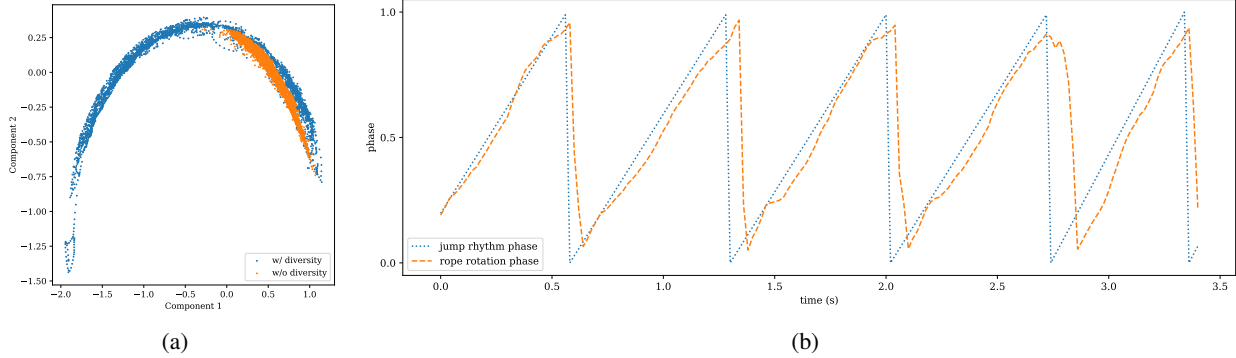


Figure 2: **Visualization Results.** (a) PCA-embedding of visited local-frame end-effector poses. (b) Plot of offset rope rotation phase and jump rhythm phase over time.

compute the target rotational angular velocity for in-place rope turning, and (2) **w/o Player Diversity**, which adopts another jumping policy trained without diversity intrinsic as counterparts during training. We use the following metrics for evaluation: (1) **Overlap Ratio**, measured as the fraction of timesteps in which the rope overlaps with the player’s OBB; (2) **Phase Tracking Error**, measured as the discrepancy between the rope rotation phase  $\hat{\theta}^{\text{rope}}$  and the derived target rotation phase  $\bar{\theta}^{\text{rope}}$ ; (3) **Player Tracking Error**, measured as the horizontal distance between the rotation center and the center of player’s OBB; and (4) **Complete Rate**, measured as the percentage of successful jumps among all attempts.

**Comparison Results** The comparison results are presented in Table 2. w/o Scheduling shows a significant performance degradation, suggesting that a simple rule-based combination cannot produce the complex cooperative behavior required for synchronized long rope skipping, where precise coordination is essential, highlighting the necessity of the proposed adaptive high-level scheduling policy. In addition, w/o Player Diversity similarly underperforms our method, indicating that introducing diverse counterparts during training is crucial for improving the generalization and adaptability of the learned coordination policy.

**Player Diversity Visualization** We further use PCA to visualize the local-frame end-effector poses visited by jumping policy with and without the diversity intrinsic objective, as shown in Figure 2a. The results show that introducing the diversity objective substantially expands the behavior distribution of the jumping policy, demonstrating its effectiveness in discovering diverse player behaviors.

**Phase Tracking Visualization** Finally, we visualize the rope rotation phase  $\bar{\theta}^{\text{rope}}$  offset by  $\frac{1-\kappa}{2}$  together with the corresponding jump rhythm phase  $\varphi$  in Figure 2b. The results indicate that two phases can stay synchronized within a small tracking error, further demonstrating the ability of the high-level scheduling policy to effectively adapt to the jumping policy.

## 5.4 Real-world Deployment

In this section, we deploy our method in four real-world scenarios listed in Figure 3. In the pure rope turning setting, our method enables two humanoids to coordinate with each other, while also allowing a single humanoid to cooperate with a human partner, demonstrating the robustness of Marope’s rope manipulation. Furthermore, when a jumping player is involved, our method successfully coordinates with both human and humanoid players, despite their large differences in jumping styles and body morphology, further confirming the strong adaptability of Marope to diverse players.

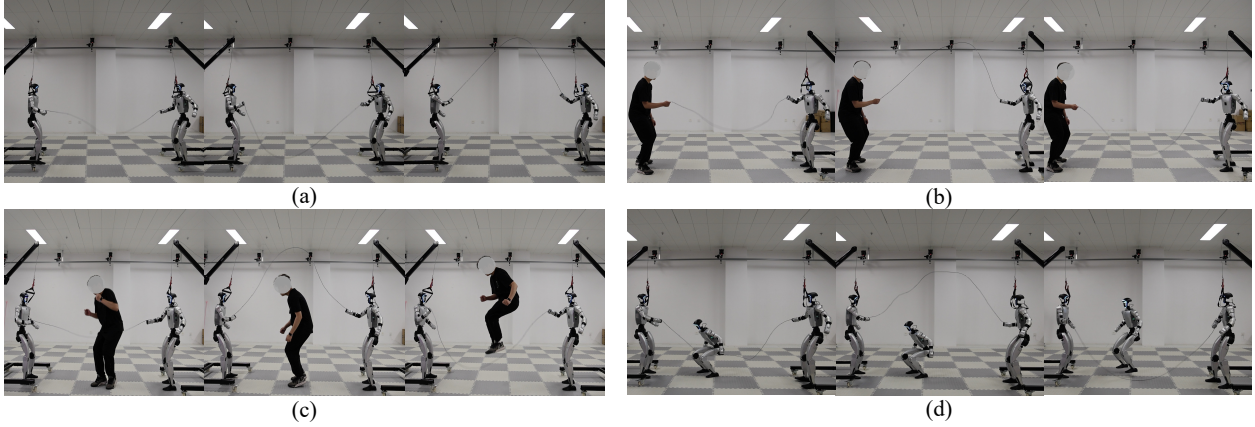


Figure 3: **Real-world Deployment.** (a) Humanoid-humanoid rope turning. (b) Humanoid-human rope turning. (c) Humanoids rope turning for a human. (d) Humanoids rope turning for a humanoid.

## 6 Conclusion

We propose Marope, a hierarchical RL framework for cooperative long rope skipping with multiple humanoid robots. Marope first learns a low-level decentralized rope manipulation policy using MAPPO. It then introduces a centralized high-level scheduling policy to follow the player’s rhythm and prevent collisions between the rope and the player. To further enhance adaptability, Marope augments the training process of high-level scheduling policy with automatically discovered diverse player behavior, improving generalization to different jumping styles. Extensive simulation and real-world experiments show that Marope achieves stable and efficient rope manipulation and can robustly cooperate with various players.

## 7 Limitations

One limitation of this work is that the proposed framework is tailored to the specific task of long rope skipping, and thus cannot be directly generalized to other cooperative humanoid tasks. Moreover, we currently focus only on a simple single-player setting, while extending the framework to multiple players and more challenging fancy rope skipping techniques (e.g. double dutch) remains an open problem. Finally, enabling humanoids to collaborate with diverse human partners in the wild via on-board sensors rather than MoCap system represents a promising direction for future work.

## References

- [Bruce et al.(2017)] Jake Bruce, Niko Sünderhauf, Piotr Mirowski, Raia Hadsell, and Michael Milford. 2017. One-shot reinforcement learning for robot navigation with interactive replay. *arXiv preprint arXiv:1711.10137* (2017).
- [Chen et al.(2026)] Yeke Chen, Shihao Dong, Xiaoyu Ji, Jingkai Sun, Zeren Luo, Liu Zhao, Jiahui Zhang, Wanyue Li, Ji Ma, Bowen Xu, et al. 2026. Learning human-like badminton skills for humanoid robots. *arXiv preprint arXiv:2602.08370* (2026).
- [Cheng et al.(2024)] Xuxin Cheng, Yandong Ji, Junming Chen, Ruihan Yang, Ge Yang, and Xiaolong Wang. 2024. Expressive whole-body control for humanoid robots. *arXiv preprint arXiv:2402.16796* (2024).
- [Crowley et al.(2023)] Devin Crowley, Jeremy Dao, Helei Duan, Kevin Green, Jonathan Hurst, and Alan Fern. 2023. Optimizing bipedal locomotion for the 100m dash with comparison to human running. In *2023 IEEE International Conference on Robotics and Automation*. IEEE, 12205–12211.
- [Di Palo and Johns(2024)] Norman Di Palo and Edward Johns. 2024. On the effectiveness of retrieval, alignment, and replay in manipulation. *IEEE Robotics and Automation Letters* 9, 3 (2024), 2032–2039.
- [Fang et al.(2023)] Yuchen Fang, Zhenggang Tang, Kan Ren, Weiqing Liu, Li Zhao, Jiang Bian, Dongsheng Li, Weinan Zhang, Yong Yu, and Tie-Yan Liu. 2023. Learning multi-agent intention-aware communication for optimal multi-order execution in finance. In *Proceedings of the 29th ACM SIGKDD Conference on Knowledge Discovery and Data Mining*. 4003–4012.
- [Feng et al.(2026)] Zhaohan Feng, Ruiqi Xue, Lei Yuan, Yang Yu, Ning Ding, Meiqin Liu, Bingzhao Gao, Jian Sun, Xihu Zheng, and Gang Wang. 2026. Multi-agent embodied ai: Advances and future directions. *Science China Information Sciences* 69, 5 (2026), 151202.
- [Guo et al.(2022)] Jun Guo, Yonghong Chen, Yihang Hao, Zixin Yin, Yin Yu, and Simin Li. 2022. Towards Comprehensive Testing on the Robustness of Cooperative Multi-Agent Reinforcement Learning. *preprint arXiv:2204.07932* (2022).
- [He et al.(2025)] Tairan He, Zhengyi Luo, Xialin He, Wenli Xiao, Chong Zhang, Weinan Zhang, Kris M Kitani, Changliu Liu, and Guanya Shi. 2025. OmniH2O: Universal and Dexterous Human-to-Humanoid Whole-Body Teleoperation and Learning. In *Conference on Robot Learning*. PMLR, 1516–1540.
- [He et al.(2024)] Tairan He, Zhengyi Luo, Wenli Xiao, Chong Zhang, Kris Kitani, Changliu Liu, and Guanya Shi. 2024. Learning human-to-humanoid real-time whole-body teleoperation. In *2024 IEEE/RSJ International Conference on Intelligent Robots and Systems*. IEEE, 8944–8951.
- [Hirai et al.(1998)] Kazuo Hirai, Masato Hirose, Yuji Haikawa, and Toru Takenaka. 1998. The development of Honda humanoid robot. In *Proceedings. 1998 IEEE international conference on robotics and automation*, Vol. 2. IEEE, 1321–1326.
- [Ji et al.(2025)] Mazeyu Ji, Xuanbin Peng, Fangchen Liu, Jialong Li, Ge Yang, Xuxin Cheng, and Xiaolong Wang. 2025. ExBody2: Advanced Expressive Humanoid Whole-Body Control. In *RSS 2025 Workshop on Whole-body Control and Bimanual Manipulation: Applications in Humanoids and Beyond*.
- [Li et al.(2019)] Tianyu Li, Hartmut Geyer, Christopher G Atkeson, and Akshara Rai. 2019. Using deep reinforcement learning to learn high-level policies on the atrias biped. In *2019 International Conference on Robotics and Automation*. IEEE, 263–269.
- [Li et al.(2021)] Zhongyu Li, Xuxin Cheng, Xue Bin Peng, Pieter Abbeel, Sergey Levine, Glen Berseth, and Koushil Sreenath. 2021. Reinforcement learning for robust parameterized locomotion control of bipedal robots. In *2021 IEEE International Conference on Robotics and Automation*. IEEE, 2811–2817.
- [Liao et al.(2025)] Qiayuan Liao, Takara E Truong, Xiaoyu Huang, Yuman Gao, Guy Tevet, Koushil Sreenath, and C Karen Liu. 2025. Beyondmimic: From motion tracking to versatile humanoid control via guided diffusion. *arXiv preprint arXiv:2508.08241* (2025).
- [Liu et al.(2023)] Fei Liu, Entong Su, Jingpei Lu, Mingen Li, and Michael C Yip. 2023. Robotic manipulation of deformable rope-like objects using differentiable compliant position-based dynamics. *IEEE Robotics and Automation Letters* 8, 7 (2023), 3964–3971.
- [Long et al.(2025)] Junfeng Long, Junli Ren, Moji Shi, Zirui Wang, Tao Huang, Ping Luo, and Jiangmiao Pang. 2025. Learning humanoid locomotion with perceptive internal model. In *2025 IEEE International Conference on Robotics and Automation*. IEEE, 9997–10003.
- [Lowe et al.(2017)] Ryan Lowe, Yi Wu, Aviv Tamar, Jean Harb, Pieter Abbeel, and Igor Mordatch. 2017. Multi-agent actor-critic for mixed cooperative-competitive environments. In *Proceedings of the 31st International Conference on Neural Information Processing Systems*. 6382–6393.

- [Mittal et al.(2025)] Mayank Mittal, Pascal Roth, James Tigue, Antoine Richard, Octi Zhang, Peter Du, Antonio Serrano-Muñoz, Xinjie Yao, René Zurbrügg, Nikita Rudin, Lukasz Wawrzyniak, Milad Rakhsha, Alain Denzler, Eric Heiden, Ales Borovicka, Ossama Ahmed, Iretyayo Akinola, Abrar Anwar, Mark T. Carlson, Ji Yuan Feng, Animesh Garg, Renato Gasoto, Lionel Gulich, Yijie Guo, M. Gussert, Alex Hansen, Mihir Kulkarni, Chenran Li, Wei Liu, Viktor Makoviychuk, Grzegorz Malczyk, Hammad Mazhar, Masoud Moghani, Adithyavairavan Murali, Michael Noseworthy, Alexander Poddubny, Nathan Ratliff, Welf Rehberg, Clemens Schwarke, Ritvik Singh, James Latham Smith, Bingjie Tang, Ruchik Thaker, Matthew Trepte, Karl Van Wyk, Fangzhou Yu, Alex Millane, Vikram Ramasamy, Remo Steiner, Sangeeta Subramanian, Clemens Volk, CY Chen, Neel Jawale, Ashwin Varghese Kuruttukulam, Michael A. Lin, Ajay Mandlekar, Karsten Patzwaltdt, John Welsh, Huihua Zhao, Fatima Anes, Jean-Francois Lafleche, Nicolas Moënné-Loccoz, Soowan Park, Rob Stepinski, Dirk Van Gelder, Chris Amevor, Jan Carius, Jumyung Chang, Anka He Chen, Pablo de Heras Ciechowski, Gilles Daviet, Mohammad Mohajerani, Julia von Muralt, Viktor Reutskyy, Michael Sauter, Simon Schirm, Eric L. Shi, Pierre Terdiman, Kenny Vilella, Tobias Widmer, Gordon Yeoman, Tiffany Chen, Sergey Grizan, Cathy Li, Lotus Li, Connor Smith, Rafael Wiltz, Kostas Alexis, Yan Chang, David Chu, Linxi "Jim" Fan, Farbod Farshidian, Ankur Handa, Spencer Huang, Marco Hutter, Yashraj Narang, Soha Pouya, Shiwei Sheng, Yuke Zhu, Miles Macklin, Adam Moravanszky, Philipp Reist, Yunrong Guo, David Hoeller, and Gavriel State. 2025. Isaac Lab: A GPU-Accelerated Simulation Framework for Multi-Modal Robot Learning. *arXiv preprint arXiv:2511.04831* (2025). <https://arxiv.org/abs/2511.04831>
- [Miyato et al.(2018)] Takeru Miyato, Toshiki Kataoka, Masanori Koyama, and Yuichi Yoshida. 2018. Spectral Normalization for Generative Adversarial Networks. In *International Conference on Learning Representations*.
- [Qi et al.(2023)] Haoxiang Qi, Xuechao Chen, Zhangguo Yu, Gao Huang, Yaliang Liu, Libo Meng, and Qiang Huang. 2023. Vertical jump of a humanoid robot with cop-guided angular momentum control and impact absorption. *IEEE Transactions on Robotics* 39, 4 (2023), 3154–3166.
- [Qin et al.(2018)] Ruilin Qin, Changle Zhou, He Zhu, Minghui Shi, Fei Chao, and Na Li. 2018. A music-driven dance system of humanoid robots. *International Journal of Humanoid Robotics* 15, 05 (2018), 1850023.
- [Radosavovic et al.(2024a)] Ilija Radosavovic, Tete Xiao, Bike Zhang, Trevor Darrell, Jitendra Malik, and Koushil Sreenath. 2024a. Real-world humanoid locomotion with reinforcement learning. *Science Robotics* 9, 89 (2024), eadi9579.
- [Radosavovic et al.(2024b)] Ilija Radosavovic, Bike Zhang, Baifeng Shi, Jathushan Rajasegaran, Sarthak Kamat, Trevor Darrell, Koushil Sreenath, and Jitendra Malik. 2024b. Humanoid locomotion as next token prediction. In *Proceedings of the 38th International Conference on Neural Information Processing Systems*. 79307–79324.
- [Rashid et al.(2018)] Tabish Rashid, Mikayel Samvelyan, Christian Schroeder, Gregory Farquhar, Jakob Foerster, and Shimon Whiteson. 2018. QMIX: Monotonic Value Function Factorisation for Deep Multi-Agent Reinforcement Learning. In *International Conference on Machine Learning*. 4295–4304.
- [Sferrazza et al.(2024)] Carmelo Sferrazza, Dun-Ming Huang, Xingyu Lin, Youngwoon Lee, and Pieter Abbeel. 2024. Humanoidbench: Simulated humanoid benchmark for whole-body locomotion and manipulation. *arXiv preprint arXiv:2403.10506* (2024).
- [Su et al.(2025)] Zhi Su, Bike Zhang, Nima Rahmanian, Yuman Gao, Qiayuan Liao, Caitlin Regan, Koushil Sreenath, and S Shankar Sastry. 2025. Hitter: A humanoid table tennis robot via hierarchical planning and learning. *arXiv preprint arXiv:2508.21043* (2025).
- [Sunehag et al.(2017)] Peter Sunehag, Guy Lever, Audrunas Gruslys, Wojciech Marian Czarnecki, Vinicius Zambaldi, Max Jaderberg, Marc Lanctot, Nicolas Sonnerat, Joel Z Leibo, Karl Tuyls, et al. 2017. Value-decomposition networks for cooperative multi-agent learning. *arXiv preprint arXiv:1706.05296* (2017).
- [Thuruthel et al.(2018)] Thomas George Thuruthel, Egidio Falotico, Mariangela Manti, and Cecilia Laschi. 2018. Stable open loop control of soft robotic manipulators. *IEEE Robotics and Automation Letters* 3, 2 (2018), 1292–1298.
- [Tong et al.(2024)] Yuchuang Tong, Haotian Liu, and Zhengtao Zhang. 2024. Advancements in humanoid robots: A comprehensive review and future prospects. *IEEE/CAA Journal of Automatica Sinica* 11, 2 (2024), 301–328.
- [Wang et al.(2022)] Xihuai Wang, Zhicheng Zhang, and Weinan Zhang. 2022. Model-Based Multi-Agent Reinforcement Learning: Recent Progress and Prospects. *preprint arXiv:2203.10603* (2022).
- [Wang et al.(2021)] Yihan Wang, Beining Han, Tonghan Wang, Heng Dong, and Chongjie Zhang. 2021. DOP: Off-Policy Multi-Agent Decomposed Policy Gradients. In *International Conference on Learning Representations*.
- [Yu et al.(2022)] Chao Yu, Akash Velu, Eugene Vinitsky, Jiaxuan Gao, Yu Wang, Alexandre Bayen, and Yi Wu. 2022. The surprising effectiveness of PPO in cooperative multi-agent games. In *Proceedings of the 36th International Conference on Neural Information Processing Systems*. 24611–24624.

- [Yuan et al.(2023)] Lei Yuan, Ziqian Zhang, Lihe Li, Cong Guan, and Yang Yu. 2023. A survey of progress on cooperative multi-agent reinforcement learning in open environment. *arXiv preprint arXiv:2312.01058* (2023).
- [Zhang et al.(2023)] Fuxiang Zhang, Chengxing Jia, Yi-Chen Li, Lei Yuan, Yang Yu, and Zongzhang Zhang. 2023. Discovering generalizable multi-agent coordination skills from multi-task offline data. In *The Eleventh International Conference on Learning Representations*.
- [Zhang et al.(2024)] Ruiqi Zhang, Jing Hou, Florian Walter, Shangding Gu, Jiayi Guan, Florian Röhrbein, Yali Du, Panpan Cai, Guang Chen, and Alois Knoll. 2024. Multi-agent reinforcement learning for autonomous driving: A survey. *arXiv preprint arXiv:2408.09675* (2024).
- [Zhang et al.(2026)] Zhikai Zhang, Haofei Lu, Yunrui Lian, Ziqing Chen, Yun Liu, Chenghui Lin, Han Xue, Zicheng Zeng, Zekun Qi, Shaolin Zheng, et al. 2026. Learning athletic humanoid tennis skills from imperfect human motion data. *arXiv preprint arXiv:2603.12686* (2026).
- [Zhu et al.(2022)] Changxi Zhu, Mehdi Dastani, and Shihan Wang. 2022. A Survey of Multi-Agent Reinforcement Learning with Communication. *preprint arXiv:2203.08975* (2022).
- [Zhuang et al.(2025)] Ziwen Zhuang, Shenzhe Yao, and Hang Zhao. 2025. Humanoid Parkour Learning. In *Conference on Robot Learning*. PMLR, 1975–1991.

**Algorithm 1** Training Procedure of Marope

**Input:** Simulation Environments  $\mathcal{E}^{\text{jump}}, \mathcal{E}^{\text{manip}}, \mathcal{E}^{\text{sched}}$ 
**Output:** Player Policy  $\pi^{\text{jump}}$ , Rope Manipulation Policy  $\pi^{\text{manip}}$ , Scheduling Policy  $\pi^{\text{sched}}$ 

- 1: **Stage I: Diverse Player Discovery**
- 2: Initialize jumping policy  $\pi^{\text{jump}}$  and metric model  $\phi$
- 3: **for** each training iteration **do**
- 4:   Roll out  $\pi^{\text{jump}}$  in  $\mathcal{E}^{\text{jump}}$
- 5:   Construct positive pairs  $\mathcal{B}^+ = \{(x_i, z_i)\}$
- 6:   Sample  $\tilde{z}_i \sim p(z)$  and construct negative pairs  $\mathcal{B}^- = \{(x_i, \tilde{z}_i)\}$
- 7:   Update  $\phi$  to maximize

$$\frac{1}{|\mathcal{B}^+|} \sum_{(x,z) \in \mathcal{B}^+} \phi(x, z) - \frac{1}{|\mathcal{B}^-|} \sum_{(x,\tilde{z}) \in \mathcal{B}^-} \phi(x, \tilde{z})$$

- 8:   Use PPO to optimize  $\pi^{\text{jump}}$  with rewards in Table 8 and diversity intrinsic  $\phi(x_i, z_i)$
- 9: **end for**
- 10:
- 11: **Stage II: Decentralized Cooperative Rope Manipulation**
- 12: Initialize rope manipulation policy  $\pi_\phi^{\text{manip}}$  with parameter sharing
- 13: **for** each training iteration **do**
- 14:   Roll out  $\pi^{\text{manip}}$  in  $\mathcal{E}^{\text{manip}}$
- 15:   Use MAPPO to optimize  $\pi_\phi^{\text{manip}}$  with rewards in Table 8
- 16: **end for**
- 17:
- 18: **Stage III: High-level Scheduling**
- 19: Load and freeze  $\pi^{\text{jump}}$  and  $\pi^{\text{manip}}$
- 20: Initialize scheduling policy  $\pi^{\text{sched}}$
- 21: **for** each training iteration **do**
- 22:   Roll out  $\pi^{\text{sched}}$  in  $\mathcal{E}^{\text{sched}}$  with  $\pi^{\text{jump}}$  and  $\pi^{\text{manip}}$
- 23:   Use PPO to optimize  $\pi^{\text{sched}}$  with rewards in Table 8
- 24: **end for**
- 25: **return**  $\pi^{\text{jump}}, \pi^{\text{manip}}, \pi^{\text{sched}}$

## A Experimental Details

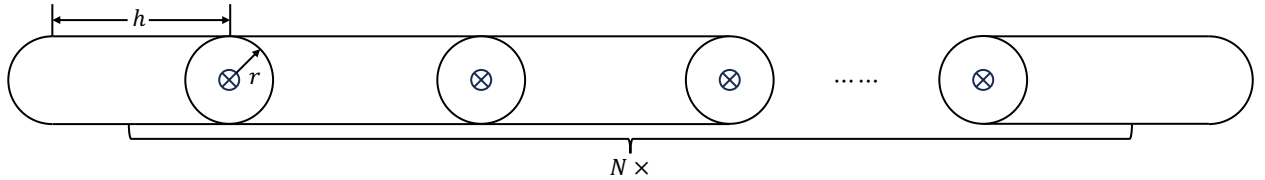


Figure 4: Schematic diagram of rope built in simulation environments.

**Simulation Environment** As illustrated in Section 5 and Figure 4, we approximate the rope as a uniform lumped multi-body system, where  $N$  rigid capsules are connected by D6 joints in Physx, the physics SDK used in Isaac Lab [Mittal et al.(2025)]. For each joint, we lock three translation DoFs to enforce local inextensibility and retain the rest three rotational DoFs to allow bending and twisting, which are applied with stiffness and damping drive properties to provide proportional passive torques. Furthermore, we assume the rope to be homogeneous and transversely isotropic. Therefore, all rigid capsules are set with the same density, all internal joints as well as two bending axes in each joint are set with the same drive properties. The default simulation parameters for rope are shown in Table 3.

**Real-world Deployment** To construct the observations of rope morphology  $o^{\text{rope}}$ , we affix 4 reflective markers on each side of the rope as shown in Figure 5, which forms 8 observable points in total to keep consistent with the design in Table 5. Similarly, when coordinating with players, we place reflective markers on players to first obtain the positions

Parameter	Value
Capsule Height ( $h$ )	0.03 m
Capsule Radius ( $r$ )	0.003 m
Capsule density	1.1 g/cm <sup>3</sup>
Bend angle limit	120°
Twist angle limit	30°
Attach offset to wrist link	0.08 m

Table 3: Default simulation parameters of rope.



Figure 5: Rope with reflective markers.

of key body parts and then compute the yaw-only OBB to form  $o^{\text{player}}$ . The rhythm signals  $\mathcal{G}^{\text{rhythm}}$  are managed by a control terminal and transported to each humanoid robot along with the MoCap information through DDS services.

## B Sim2Real Transfer

Table 4 presents the dynamics randomization techniques and observation noises used in Marope. For each humanoid robot, we randomize its physical materials, body mass and center of mass in torso link and apply random push on base link. For discretely simulated rope, we randomize its length, density and internal drive properties. The observation terms that require on-board sensing or external MoCap streaming are injected with corresponding noises.

## C Training Details

Algorithm 1 displays the whole training procedure of Marope in different stages, where Line 1-9 shows the interleaved optimization on  $\pi^{\text{jump}}$  and  $\phi$  in Section 4.3, Line 11-16 presents the multi agent policy optimization on  $\pi^{\text{manip}}$  in Section 4.1 and Line 18-24 corresponds to the high-level coordination in Section 4.2. The training hyperparameters are summarized in Table 5 6 7.

## D Reward Design

Table 8 lists the detailed reward terms designed for specific policy in Marope. Specifically, for low-level rope manipulation, four main reward terms are used to guide policy  $\pi^{\text{manip}}$  to follow the command  $\mathcal{G}^{\text{manip}}$ . Additional regularization terms penalize wrong facing direction, unstable control and overall poses. For high-level scheduling, besides the phase tracking reward mentioned in Section 4.2, we also introduce an auxiliary shaping reward for rope to rotate under the clock frequency for faster convergence. The player tracking reward and overlap penalty incentivize  $\pi^{\text{sched}}$  to adapt to the slight horizontal drift of player and reduce the rope-player collision. For player jumping policy training, a single rhythm alignment reward is enough to derive the periodic jumping behavior as described in Section 4.2. To prevent weird motion style when adding diversity intrinsic, the rest regularization terms further constrains the feet distance, joint symmetry, feet contact force, etc.

Table 4: Sim2Real transfer strategies in Marope.

	Term	Value
<b>Dynamics Randomization</b>	<i>Rope</i>	
	Number of rigid capsules ( $N$ )	$\mathcal{U}(80, 100)$
	Capsule density	$\mathcal{U}(0.8, 1.2) \times \text{default}$
	Bend stiffness coefficient	$\mathcal{U}(10.0, 40.0)$
	Bend damping coefficient	$\mathcal{U}(2.0, 10.0)$
	Twist stiffness coefficient	$\mathcal{U}(4.0, 16.0)$
	Twist damping coefficient	$\mathcal{U}(1.0, 5.0)$
	<i>Humanoid</i>	
	Static friction coefficient	$\mathcal{U}(0.3, 1.6)$
	Dynamic friction coefficient	$\mathcal{U}(0.3, 1.2)$
	Restitution coefficient	$\mathcal{U}(0.0, 0.5)$
	Body link mass	$\mathcal{U}(0.9, 1.1) \times \text{default}$
	Torso CoM offset	$\mathcal{U}([-0.025, 0.025], [-0.05, 0.05], [-0.05, 0.05])$ m
	Push robot velocities	$v_x, v_y \in \mathcal{U}(-0.5, 0.5)$ m/s
Push robot interval	$\mathcal{U}(1.0, 3.0)$ s	
<b>Observations Noise</b>	<i>Proprioception</i>	
	Projected gravity	$\mathcal{U}(-0.05, 0.05)$
	Base angular velocity	$\mathcal{U}(-0.2, 0.2)$
	Joint position	$\mathcal{U}(-0.01, 0.01)$
	Joint velocity	$\mathcal{U}(-0.5, 0.5)$
	<i>Rope Morphology</i>	
	Segment position	$\mathcal{U}(-0.1, 0.1)$
	<i>Player</i>	
	OBB position	$\mathcal{U}(-0.1, 0.1)$
	6D OBB orientation	$\mathcal{U}(-0.05, 0.05)$
	OBB size	$\mathcal{U}(-0.1, 0.1)$

Table 5: Training hyperparameters of low-level rope manipulation policy.

Category	Hyperparameter	Value
<b>Architecture</b>	Policy MLP hidden dimensions	[512, 256, 128]
	Critic MLP hidden dimensions	[512, 256, 128]
	Activation function	ELU
	Policy distribution	Gaussian
	Policy std range	(0.1, 2.0)
	Observation history ( $H$ )	5
	Observable points on rope ( $m$ )	8
<b>Training</b>	Steps per environment	25
	Learning rate ( $\eta$ )	$3 \times 10^{-4}$
	Max gradient norm ( $\ \mathbf{g}\ _{\text{clip}}$ )	1.0
	Clip parameter	0.2
	Entropy coefficient	0.01
	Value loss coefficient	1.0
	Discount factor ( $\gamma$ )	0.99
	GAE $\lambda$	0.95
	Desired KL	0.01
	Learning epochs	5
Mini-batches	4	

Table 6: Training hyperparameters of high-level scheduling policy.

Category	Hyperparameter	Value
<b>Architecture</b>	Policy MLP hidden dimensions	[256, 128, 64]
	Critic MLP hidden dimensions	[256, 128, 64]
	Activation function	ELU
	Policy distribution	Beta
	Concentration range	[0.1, 25.0]
	Observation history ( $H$ )	5
<b>Training</b>	Steps per environment	25
	Learning rate ( $\eta$ )	$3 \times 10^{-4}$
	Max gradient norm ( $\ \mathbf{g}\ _{\text{clip}}$ )	1.0
	Clip parameter	0.2
	Entropy coefficient	0.01
	Value loss coefficient	1.0
	Discount factor ( $\gamma$ )	0.99
	GAE $\lambda$	0.95
	Desired KL	0.01
	Learning epochs	5
	Mini-batches	4

Table 7: Training hyperparameters of diverse player jumping policy.

Category	Hyperparameter	Value
<b>Architecture</b>	Policy MLP hidden dimensions	[512, 256, 128]
	Critic MLP hidden dimensions	[512, 256, 128]
	Metric MLP hidden dimensions	[256, 128, 64]
	Activation function	ELU
	Latent command dimension ( $d_{\text{latent}}$ )	4
	Policy distribution	Gaussian
	Standard derivation range	(0.1, 2.0)
	Observation history ( $H$ )	10
<b>Training</b>	Steps per environment	25
	Learning rate ( $\eta$ )	$3 \times 10^{-4}$
	Max gradient norm ( $\ \mathbf{g}\ _{\text{clip}}$ )	1.0
	Clip parameter	0.2
	Entropy coefficient	0.01
	Value loss coefficient	1.0
	Discount factor ( $\gamma$ )	0.99
	GAE $\lambda$	0.95
	Desired KL	0.01
	Learning epochs	5
Mini-batches	4	
Task reward threshold for diversity intrinsic	0.3	
Diversity intrinsic weight ( $\beta$ )	1.0	

Table 8: Reward terms for different policy training in Marope.

	Term	Expression	Weight	
	<i>Task Objectives</i>			
	Track linear velocity	$\exp(-8.0 \ \mathbf{v}_{xy}^c - [\hat{v}_x^{\text{lin}}, \hat{v}_y^{\text{lin}}]\ _2^2)$	2.0	
	Track angular velocity	$\exp(-8.0 \ \omega_z^r - \hat{v}_z^{\text{ang}}\ _2^2)$	2.0	
	Track width	$\exp(-20.0 \ \mathbf{p}_{xy}^{\text{end}} - \mathbf{p}_{xy}^{\text{start}}\ _2 - \hat{w})$	1.0	
	Track rotation	$\exp(-0.04 \ \bar{\omega} - \hat{\omega}\ _2^2)$	4.0	
	<i>Regularization</i>			
<b>Low-level Rope Manipulation</b>	Face to other	$\ \Delta\theta_{\text{facing}} \cdot \mathbf{1}(\Delta\theta_{\text{facing}} < \frac{\pi}{12})\ _2^2$	-1.0	
	Action rate	$\ a_t - a_{t-1}\ _2^2$	-0.05	
	Flat orientation	$\ \mathbf{g}_{xy}^b\ _2^2$	-5.0	
	Angular velocity in $xy$	$\ \omega_{xy}^b\ _2^2$	-0.05	
	Joint position limits	$\sum_i [\mathbf{1}(\mathbf{q}_i \geq \mathbf{q}_i^{\text{upper}}) + \mathbf{1}(\mathbf{q}_i \leq \mathbf{q}_i^{\text{lower}})]$	-10.0	
	Joint deviation (upper body)	$\sum_{i \in \mathcal{U}}  \mathbf{q}_i - \mathbf{q}_i^{\text{default}} $	-0.05	
	Joint deviation (waist)	$\sum_{i \in \mathcal{W}}  \mathbf{q}_i - \mathbf{q}_i^{\text{default}} $	-0.1	
	Joint deviation (lower body)	$\sum_{i \in \mathcal{L}}  \mathbf{q}_i - \mathbf{q}_i^{\text{default}} $	-0.1	
	Slide with contact	$\sum_k \ \mathbf{v}_{xy}^{\text{foot}_k, t}\ _2 \mathbf{1}(\text{foot}_k \text{ contacts})$	-0.4	
	Undesired contacts	$\mathbf{1}(\text{non-foot bodies contact})$	-1.0	
		<i>Task Objectives</i>		
	<b>High-level Scheduling</b>	Track frequency	$\exp(-1.5 (\ \bar{\omega}\  / 2\pi - \nu)^2)$	1.0
Track phase		$\exp(-1.0 \ \bar{\theta}^{\text{rope}} - \hat{\theta}^{\text{rope}}\ _2^2)$	1.0	
Track player		$\exp(-4.0 \ \mathbf{p}_{xy}^c - \mathbf{p}_{xy}^{\text{player}}\ _2^2)$	1.0	
Overlap		$\mathbf{1}(\exists k, \mathbf{p}_t^{\text{rope}}[k] \in \text{OBB}_{\text{player}})$	-1.0	
Command rate		$\ \mathbf{u}_t - \mathbf{u}_{t-1}\ _2^2, \mathcal{G}_t^{\text{manip}} = \text{affine}(\mathbf{u}_t)$	-0.2	
	<i>Task Objectives</i>			
	Align rhythm	$(2 \cdot \mathbf{1}(\text{contact} = c) - 1)(0.8 \cdot \mathbf{1}(c = 1) + 0.2 \cdot \mathbf{1}(c = 0))$	8.0	
	<i>Regularization</i>			
<b>Player</b>	Feet distance	$d_{\text{feet}} - \text{clip}(d_{\text{feet}}, 2.5, 4)$	-2.0	
	Reduce linear velocity	$\exp(-1.5 \ \mathbf{v}_{xy}^{\text{base}}\ _2^2)$	1.0	
	Reduce angular velocity	$\exp(-2.0 \ \omega_z^{\text{base}}\ _2^2)$	1.0	
	Action rate	$\ \mathbf{a}_t - \mathbf{a}_{t-1}\ _2^2$	-0.05	
	Angular velocity in $xy$	$\ \omega_t^{xy}\ _2^2$	-0.05	
	Joint position limits	$\sum_i [\mathbf{1}(\mathbf{q}_i \geq \mathbf{q}_i^{\text{upper}}) + \mathbf{1}(\mathbf{q}_i \leq \mathbf{q}_i^{\text{lower}})]$	-10.0	
	Joint deviation (upper body)	$\sum_{i \in \mathcal{U}}  \mathbf{q}_i - \mathbf{q}_i^{\text{default}} $	-0.1	
	Joint deviation (waist)	$\sum_{i \in \mathcal{W}}  \mathbf{q}_i - \mathbf{q}_i^{\text{default}} $	-0.8	
	Joint deviation (lower body)	$\sum_{i \in \mathcal{L}}  \mathbf{q}_i - \mathbf{q}_i^{\text{default}} $	-0.5	
	Joint mirror (upper body)	$\ \mathbf{q}_{\text{upper}}^{\text{L}} - \mathbf{q}_{\text{upper}}^{\text{R}}\ _2^2$	-0.2	
	Joint mirror (lower body)	$\ \mathbf{q}_{\text{lower}}^{\text{L}} - \mathbf{q}_{\text{lower}}^{\text{R}}\ _2^2$	-0.2	
	Feet contact force	$\left  \text{clip}\left(\frac{\mathbf{F}_{\text{z}}^{\text{feet}}}{m_{\text{body}}} - 2.5g, 0, \infty\right) \right _2$	-0.1	
	Slide with contact	$\sum_k \ \mathbf{v}_{xy}^{\text{foot}_k, t}\ _2 \mathbf{1}(\text{foot}_k \text{ contacts})$	-0.5	
Undesired contacts	$\mathbf{1}(\text{non-foot bodies contact})$	-1.0		